Analysis of Thick Microstrip Antennas by the Meshfree Collocation Method

B. Honarbakhsh[1] and A. Tavakoli[1, 2]

[1]Department of Electrical Engineering
[2]Institute of Communications Technology and Applied Electromagnetics
Amirkabir University of Technology (Tehran Polytechnic), Tehran, IRAN
b_honarbakhsh@aut.ac.ir and tavakoli@aut.ac.ir

Abstract ─ A meshless integration free approach is applied to numerical solution of the mixed potential integral equation (MPIE) governing various microstrip resonators/antennas. The idea behind the discrete complex image method (DCIM) is exploited to provide closed form expressions for all of the integrals, leading to an efficient spectral-domain meshless integral equation (IE) solver. The proposed meshfree method (MFM) is compared with low order method of moments (MoM) from the aspects of memory usage and simulation time, which shows superior performance of the MFM.

Index Terms - Collocation, meshfree, microstrip antenna, MoM, RBF, and Shepard.

I. INTRODUCTION

Currently, meshfree methods (MFMs) are well-known as partial differential equation (PDE) solvers and the amount of research devoted to meshless solution of integral equations (IEs) is negligible [1-7]. Not so far, a study is reported on numerical solution of electromagnetic (EM) IEs by the meshfree collocation method (MCM) [7]. The purpose of this work is applying that method to the analysis of microstrip resonators/antennas by meshfree (meshless) solution of the mixed potential integral equation (MPIE) [8]. This equation is the most practical IE in numerical solution of microstrip structures due to its weak singular kernels, numerical stability, and intense capability of handling multilayered media [9].

At present, the method of moments (MoM) is known as the most versatile numerical method for such problems. One of the pre-assumptions in MoM is partitioning the problem domain by meshes. The unknown field variable is then expanded over known basis functions with unknown weightings on each mesh, leading to discretization of the IE. These expansion functions most often have simple mathematical form and thus, low reconstruction capability. Although it is possible to use basis functions with high reconstruction ability, currently the most used MoM solvers are of low order. Hereafter in this paper, by MoM it is meant low order MoM, which exploits pulse/roof-top basis functions.

In contrast to MoM, MFMs discretize operator equations by nodes instead of meshes and utilizing meshfree shape functions. These functions are highly complicated, with excellent fitting capability [10]. Thus, it is expected that MFMs be able to solve the same problem with less number of unknowns compared to MoM, leading to save in memory usage. On the other hand, noting that evaluation of meshless shape functions often requires matrix computations, MFMs are expected to be slow solvers. This makes meshless solution of IEs a challenging problem.

For decreasing the simulation time, guidelines reported in [7] are followed throughout this paper, which has led to less computational cost with respect to MoM. Since all numerical integrations are effectively carried out in the spectral domain, the proposed method can be regarded as the meshless counterpart of the spectral domain MoM. This study covers different aspects of geometries, feeding techniques, nature of structures, and number of exciting ports. For decoupling the effect of the substrate Green's functions (GFs) from the

method itself, the first four structures are analyzed based of air-filled substrate and for completeness, the last case is devoted to a realistic antenna.

All MFM simulations are carried out based on regular node arrangements. This restriction is due to presently available strategy for bypassing numerical integration. By introducing wise irregularity in node distribution, the scattered data fitting capability of meshless shape functions can be exploited which leads to more decrease in the number of unknowns. Nevertheless, although the present study has led to over sampling of the problem domain, both of the number of unknowns and simulation time are decreased compared to MoM. The main ideas of the method are general and can be applied to arbitrary node arrangements. Finally, it should be pointed out that by "thick" we mean that the variations of EM fields normal to the substrate are not neglected in this work.

II. MATHEMATICAL STATEMENT OF THE PROBLEM

Consider a planar microstrip structure of domain Ω and boundary $\partial\Omega$, illuminated by an incident electric field, $\mathbf{E}^i$. The MPIE governing this problem can be expressed as

$$\begin{cases} \mathbf{n} \times \mathbf{E}^i = \mathbf{n} \times \left(j\omega\mathbf{A} + \nabla V \right), \text{ in problem domain} \\ \mathbf{m} \cdot \mathbf{J}_s = 0, \text{ on smooth boundaries} \\ \mathbf{J}_s = 0, \text{ on convex corners} \end{cases} \quad (1)$$

where $\mathbf{n}$ and $\mathbf{m}$ are unit normal vectors to Ω and $\partial\Omega$, respectively, with $\mathbf{n} \cdot \mathbf{m} = 0$. In addition

$$\begin{cases} \mathbf{A}(\boldsymbol{\rho}) = \mu_0 \int_\Omega \overline{\overline{\mathbf{G}}}_A (\boldsymbol{\rho}, \boldsymbol{\rho}') \cdot \mathbf{J}_s (\boldsymbol{\rho}') d\Omega \\ \varepsilon_0 V(\boldsymbol{\rho}) = \int_\Omega G_V (\boldsymbol{\rho}, \boldsymbol{\rho}') \rho_s (\boldsymbol{\rho}') d\Omega \end{cases} \quad (2)$$

where $\overline{\overline{\mathbf{G}}}_A$ and G_V are dyadic and scalar GFs of the substrate medium, respectively [9]. As well, ρ_s and $\mathbf{J}_s$ are related by the continuity equation, i.e.,

$$\nabla \cdot \mathbf{J}_s + j\omega\rho_s = 0. \quad (3)$$

In conventional MoM solvers, $\mathbf{J}_s$ is expanded over a set of basis functions satisfying boundary conditions (BCs) and equation (2) is injected in equation (1). Thus, the problem reduces to

$$\varepsilon_0 \mathbf{n} \times \mathbf{E}^i (\boldsymbol{\rho}) = \mathbf{n} \times \left[j\omega\varepsilon_0\mu_0 \int_\Omega \overline{\overline{\mathbf{G}}}_A (\boldsymbol{\rho}, \boldsymbol{\rho}') \cdot \mathbf{J}_s (\boldsymbol{\rho}') d\Omega \right.$$
$$\left. + \nabla \int_\Omega G_V (\boldsymbol{\rho}, \boldsymbol{\rho}') \rho_s (\boldsymbol{\rho}') d\Omega \right], \quad (4)$$

and is solved by a weighted residual method, which is usually of the Galerkin type. This choice with applying integration by parts, removes the gradient operator [9]. As the MoM enforces the basis functions to be only linear independent, it is possible to use simple functions such as rectangular pulses and roof-tops. These functions have low order of continuity, and therefore, differentiation is not straightforward, if not impossible. On the other hand, this option simplifies computing of fourfold integrals appearing in solution of 2D problems.

In contrast to MoM, MFM not only enforces the meshless shape functions to be linear independent, but also imposes them to be either approximants or interpolants. Sample 1D approximant and interpolant meshless shape functions are depicted in Fig. 1.
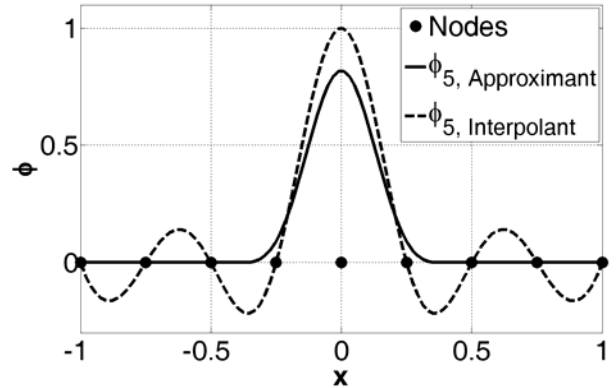
Fig. 1. Sample 1D approximant and interpolant meshless shape functions.

Clearly, construction of meshless shape functions satisfying the BCs of equation (1) is too hard, if not impossible. As stated earlier, these functions possess high order of continuity and their evaluation is computationally expensive. Thus, numerical integration over them is time consuming, which makes application of the Galerkin method computationally inefficient. As a conclusion, for meshless solution of the MPIE, we suggest the collocation method, without replacing equation (2) into equation (1).

III. MESHLESS DISCRETIZATION

The first step for meshless discretization is to scatter M nodes in the problem domain and on its boundary. This leads to nodal description of the problem. Next, the unknown field variable should be expanded over meshless shape functions. This step is highly problem dependent. An improper selection of expansion functions leads to inaccuracy and/or computational inefficiency. Considering the present formulation, i.e., equations (1) and (2), reveals that the problem can be regarded as a combination of two parts; the differential part, i.e., equation (1), and an integral part, i.e., equation (2). Thus, the field variable V should be expanded over a set of smooth functions; no matter they are localized or distributed over the entire problem domain. We suggest expanding V over radial basis function (RBF) interpolants and not over moving least square (MLS) approximants. For detailed introduction to meshless shape functions, the reader is referred to [10]. The relative computational cost of evaluating the differential part for a sample 2D problem is reported in Fig. 2, wherein conventional MLS and RBF shape functions are used.
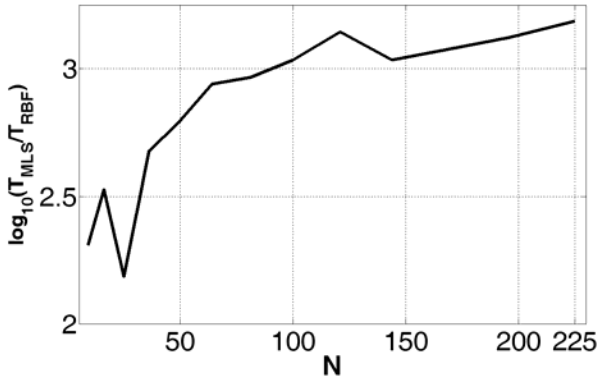
Fig. 2. Relative computational cost of evaluating the differential part for a sample 2D problem.

On the other hand, $\mathbf{J}_s$ should be expanded over functions, which are localized over a small portion of the problem domain. If not, integration over each of the corresponding shape functions requires either huge number of quadrature points or a back ground mesh. The computational cost of evaluating the integral part for a sample 2D problem using conventional MLS, Shepard and RBF shape functions is reported in Fig. 3. Thus, we suggest expanding $\mathbf{J}_s$ over Shepard

approximants [11], which their evaluation does not require matrix computations.
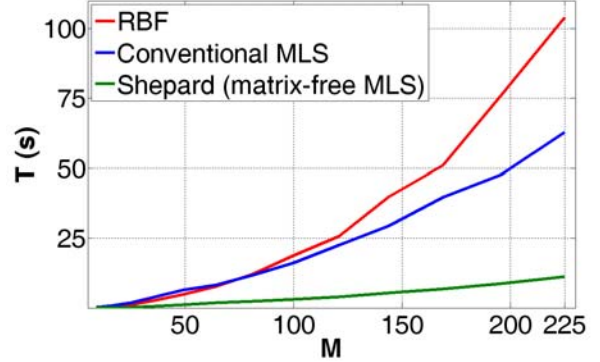
Fig. 3. Computational cost of evaluating the integral part for a sample 2D problem using different meshless shape functions.

Assume $\{\varphi_i\}_{i=1}^{M}$ and $\{\psi_i\}_{i=1}^{M}$ be sets of, respectively, interpolants and approximants corresponding to nodes describing the problem. Therefore,

$$\begin{cases} V^h(\boldsymbol{\rho}) = \boldsymbol{\Phi}^T(\boldsymbol{\rho}) \cdot \widehat{\mathbf{V}} = \sum_{i=1}^{M} \varphi_i(\boldsymbol{\rho}) \widehat{V}_i \\ A_\alpha^h(\boldsymbol{\rho}) = \boldsymbol{\Phi}^T(\boldsymbol{\rho}) \cdot \widehat{\mathbf{A}_\alpha} = \sum_{i=1}^{M} \varphi_i(\boldsymbol{\rho}) \widehat{A_{\alpha,i}}, \\ J_\alpha^h(\boldsymbol{\rho}) = \boldsymbol{\Psi}^T(\boldsymbol{\rho}) \cdot \widehat{\mathbf{J}_\alpha} = \sum_{i=1}^{M} \psi_i(\boldsymbol{\rho}) \widehat{J_{\alpha,i}} \end{cases} \quad (5)$$

with

$$\begin{cases} \widehat{\mathbf{V}} = \begin{bmatrix} \widehat{V}_1 & \dots & \widehat{V}_M \end{bmatrix}^T \\ \widehat{\mathbf{A}_\alpha} = \begin{bmatrix} \widehat{A_{\alpha,1}} & \dots & \widehat{A_{\alpha,M}} \end{bmatrix}^T, \\ \widehat{\mathbf{J}_\alpha} = \begin{bmatrix} \widehat{J_{\alpha,1}} & \dots & \widehat{J_{\alpha,M}} \end{bmatrix}^T \end{cases} \quad (6)$$

where V^h and A_α^h are interpolated value of V and A_α, respectively, J_α^h is the approximated value of J_α, and α is either of x or y. Collocating sides of equation (5) and the first of equation (1) at the nodes yields

$$\mathbf{L} \cdot \hat{\mathbf{J}} = \mathbf{b}, \quad (7)$$

where

$$\begin{cases} \mathbf{L} = \begin{bmatrix} \mathbf{L}_{11} & \mathbf{L}_{12} \\ \mathbf{L}_{21} & \mathbf{L}_{22} \end{bmatrix} \\ \hat{\mathbf{J}}^T = \begin{bmatrix} \widehat{\mathbf{J}}_x^T & | & \widehat{\mathbf{J}}_y^T \end{bmatrix} \\ \mathbf{b}^T = \begin{bmatrix} E_{x,1}^i \cdots E_{x,M}^i | E_{y,1}^i \cdots E_{y,M}^i \end{bmatrix} \end{cases} \quad (8)$$

with

$$\begin{cases} \mathbf{L}_{11} = j\omega\mu_0\mathbf{K}_1 - \left(j\omega\varepsilon_0\right)^{-1}\boldsymbol{\Phi}_x \cdot \mathbf{K}_2 \\ \mathbf{L}_{12} = -\left(j\omega\varepsilon_0\right)^{-1}\boldsymbol{\Phi}_x \cdot \mathbf{K}_3 \\ \mathbf{L}_{21} = -\left(j\omega\varepsilon_0\right)^{-1}\boldsymbol{\Phi}_y \cdot \mathbf{K}_2 \\ \mathbf{L}_{22} = j\omega\mu_0\mathbf{K}_1 - \left(j\omega\varepsilon_0\right)^{-1}\boldsymbol{\Phi}_y \cdot \mathbf{K}_3 \end{cases}, \qquad (9)$$

and

$$\begin{cases} \left[\mathbf{K}_1\right]_{ij} = \int_{\Omega}\psi_j\left(\boldsymbol{\rho}'\right)G_A^{xx}\left(\boldsymbol{\rho}_i,\boldsymbol{\rho}'\right)d\Omega \\ \left[\mathbf{K}_2\right]_{ij} = \int_{\Omega}\psi_{j,x}\left(\boldsymbol{\rho}'\right)G_V\left(\boldsymbol{\rho}_i,\boldsymbol{\rho}'\right)d\Omega. \\ \left[\mathbf{K}_3\right]_{ij} = \int_{\Omega}\psi_{j,y}\left(\boldsymbol{\rho}'\right)G_V\left(\boldsymbol{\rho}_i,\boldsymbol{\rho}'\right)d\Omega \end{cases} \qquad (10)$$

The unknown field variable $\hat{\mathbf{J}}$ can now be computed by solving the linear system of equation (7) after imposition of BCs, which is now straightforward.

IV. COMPUTATION OF THE L MATRIX

This section follows [7]. The computational cost of the **L** matrix is mainly due to matrices introduced in equation (10). The key point is noting the fact that under the assumption of regular node arrangement, Shepard functions become bell-shaped and consequently, can be well approximated by a single Gaussian function. Hereafter, we assume

$$\psi_i\left(x + x_i, y + y_i\right) = \exp\left[-\left(\xi_x^{(i)}x^2 + \xi_y^{(i)}y^2\right)\right], \qquad (11)$$

where a_i, $\xi_x^{(i)}$ and $\xi_y^{(i)}$ are constants corresponding to the ith approximant and can be simply estimated by curve fitting methods. This point, itself, simplifies handling the problem and increases computational efficiency. The aforementioned matrices can be computed in both of space and spectral domains. Thus, we split this section to two parts and discuss each one separately.

A. Space domain

Computation in the space domain requires evaluation of space domain GFs of the problem. Although the GFs of multi-layered media have closed forms in the spectral domain, their evaluation in the space domain has a long history and still is known as an active research topic. Currently, one of the most famous and efficient approaches used for this purpose, is the discrete complex image method (DCIM) [12, 13]. The DCIM is a general idea for computing the inverse

Fourier-Bessel transform and, itself, can be implemented in a variety of ways. In this work, we have followed [13] which, for the problem at hand, express the space domain GFs as a sum of complex-valued spherical wave, i.e.,

$$\begin{cases} G\left(\boldsymbol{\rho},\boldsymbol{\rho}'\right) = \sum_{p=1}^{P}c_p\dfrac{e^{-jk_0r_p}}{4\pi r_p} \\ r_p = \sqrt{\left|\boldsymbol{\rho}-\boldsymbol{\rho}'\right|^2 - d_p^2} \end{cases}, \qquad (12)$$

where $c_m, d_m \in \mathbb{C}$ and $G = G_A^{xx}, G_A^{yy}, G_V$. Details of this method are beyond the scope of this work. Considering equations (10) to (12), the mathematical form of the first integrals in equation (10) can be stated as

$$\begin{cases} f\left(m,n\right) = \int_{\Omega_n}f_m\left(x,y\right)f_n\left(x,y\right)d\Omega \\ f_m\left(x+x_m, y+y_m\right) = \dfrac{\exp\left[-jk_0\sqrt{x^2+y^2-d_p^2}\right]}{\sqrt{x^2+y^2-d_p^2}}, \\ f_n\left(x+x_n, y+y_n\right) = \exp\left[-\left(\xi_x^{(n)}x^2 + \xi_y^{(n)}y^2\right)\right] \end{cases} \qquad (13)$$

where Ω_n is the support of the nth approximant. The other integrals can be stated, and consequently treated similarly. This integral has a potential first order singularity and is classified as a weak singular integral. Nevertheless, for fast and accurate numerical integration, all sharp behaviours and infinite values of the integrand should be avoided. Such integrals can be evaluated numerically by applying the Duffy transform, which is simple to implement and annihilates the possible singularity at the expense of triangular meshing the integration domain and the corresponding increase in computational complexity [14].

B. Spectral domain

It is well known that all integrals of equation (10) are linear convolutions. This fact can be exploited to calculate equation (10) by the continuous Fourier transform (CFT), e.g., the jth column of $\mathbf{K}_1$ can be computed as follows

$$\left[\mathbf{K}_1\right]_{ij} = \mathcal{F}^{-1}\left\{\mathcal{F}\left\{\psi_j\right\}\cdot\mathcal{F}\left\{G_A^{xx}\right\}\right\}, \quad i=1,...,M, \qquad (14)$$

where $\mathcal{F}$ stands for CFT. A situation exists, which can decrease the computational cost of the method by providing closed form expressions for the integrals of equation (10). Suppose,

$$\begin{cases} \psi_i(\boldsymbol{\rho}) = \psi(\boldsymbol{\rho} - \boldsymbol{\rho}_i) \\ \xi_x^{(i)} = \xi_y^{(i)} = \xi \end{cases}, \quad 1 \le i \le M \qquad (15)$$

which is met by nodal arrangements with equal radial distance. Thus, the mathematical forms of the required integrals are

$$\begin{cases} g_1(\boldsymbol{\rho}) = \int_0^\infty e^{-\frac{k_\rho^2}{4\xi}} \widetilde{G_A^{xx}}(k_\rho^2) J_0(k_\rho\rho) k_\rho dk_\rho \\ g_2(\boldsymbol{\rho}) = \cos\varphi \int_0^\infty e^{-\frac{k_\rho^2}{4\xi}} \widetilde{G_V}(k_\rho^2) J_1(k_\rho\rho) k_\rho^2 dk_\rho, \\ g_3(\boldsymbol{\rho}) = \sin\varphi \int_0^\infty e^{-\frac{k_\rho^2}{4\xi}} \widetilde{G_V}(k_\rho^2) J_1(k_\rho\rho) k_\rho^2 dk_\rho, \end{cases} \quad (16)$$

where $\widetilde{G}$ stands for the spectral domain counterpart of G. The remained step is computing the above Sommerfeld-type integrals, which can be done by following the strategy introduced in [13]. The time gain achieved by computing the first integral of equation (16) in space and spectral domains for a sample 2D problem is reported in Fig. 4. Relaxing the condition of equation (15) does not invalidate this approach. Application to general case is under study.
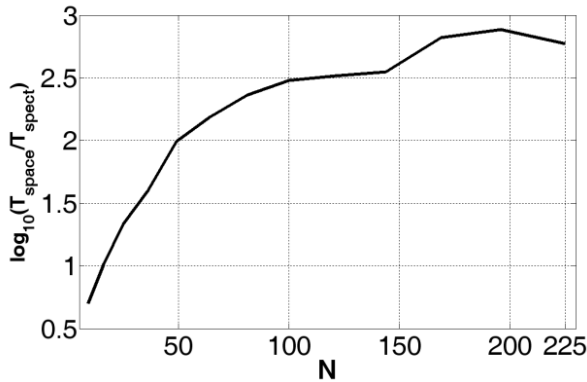
Fig. 4. Time gain achieved by computing the first integral of equation (16) in space and spectral domains.

V. FEED MODELING

There are varieties of methods for feeding microstrip antennas [9, 15]. One of the most practical picks is to directly connect a microstrip line to the radiating patch. This choice has two valuable benefits. First, it preserves the planarity of the problem and restricts the discretization to the microstrip plane. Second, it allows analysis of the problem by the collocation method. This is in contrast to feeding by vertical filament acting on some point of the upper conductor, which requires a distributed weighting function needed for absorbing the singularity of the Dirac delta function. Another choice is proximity feeding technique, in which the feed line truncates at the vicinity of the radiating element. Although this case preserves benefits of the former one, the coupling of EM energy is drastically decreased compared to that, making the impedance matching difficult. Moreover, the high sensitivity of the return loss to the distance between the line and patch makes this choice impractical. Nevertheless, from numerical stand point and for the purpose of validation, both of the aforementioned methods are used in this study.

Another point that should be noted is the mathematical form of the excitation function. In MoM, it is straightforward to use a half roof-top function with acting at the first mesh of the feed line. In this case the EM field distribution of the exciting function suddenly drops from its maximum value to zero. This sharp variation does not affect the solution and satisfactory results are obtained following this strategy. We have found that meshless methods are incapable of handling abrupt changes. In fact, we could not get satisfactory results from the proposed method unless we modeled the excitation by a smooth decaying function. In this study, a slowly decaying Gaussian function is used. At present, the optimum value for the damping factor is unknown to us.

VI. NUMERICAL DE-EMBEDDING

A crucial step in both of the measurement and numerical analysis of microwave components is extracting the scattering (S) parameters. The difficulty of this step arises from the disturbance of the EM field at the source/load location. The process of extracting the effect of the source/load from the intrinsic behavior of the component is called de-embedding. In the context of numerical solution, this problem resembles itself, specially, when dealing with IE solvers and is called numerical de-embedding. Number of strategies is introduced for this purpose, e.g., [16, 17]. In this work, we followed [17]; it is simple and does not need knowledge of characteristic impedance of the feed line and its guiding wave length.

VII. NUMERICAL RESULTS

In this section, the proposed method is applied to five microstrip structures: a linear resonator, a proximity-coupled circular resonator, a proximity-coupled antenna array, a line-fed dual-polarized patch antenna, and a line-fed patch antenna. One of the vital steps in such analysis is evaluating of integrals including GFs of layered media. Any error in this step, directly affects the final result. Thus, for decoupling the effect of GFs from the method, the first four problems are devoted to substrates with $\varepsilon_r = 1$. These problems prove the capability of the method in handling various geometries and different feeding techniques. The final problem is a realistic microstrip antenna with $\varepsilon_r = 2.2$. The MFM analysis is based on the proposed spectral domain strategy. Apparently, it is also possible to evaluate the coefficient matrix by direct numerical integration in the space domain.

Meshless interpolants are constructed by the following compactly supported positive definite RBF [10],

$$R(\boldsymbol{\rho}) = \begin{cases} (1-\eta)^5 \\ \times (8 + 40\eta + 48\eta^2 + 25\eta^3 + 5\eta^4), & 0 \leq \eta \leq 1 \\ 0, & \eta > 1 \end{cases}$$

(17)

where $\eta = \rho/r_I$, with r_I being the interpolant support size. For the first four problems $r_I = 30d_r$, and for the last one $r_I = 10d_r$ where d_r is the radial nodal distance. As well, Shepard approximants are constructed from the following quadric spline function [10],

$$w(\boldsymbol{\rho}) = \begin{cases} 1 - 6\eta^2 + 8\eta^3 - 3\eta^4, & 0 \leq \eta \leq 1 \\ 0, & \eta > 1 \end{cases}$$

(18)

where $\eta = \rho/r_A$, with r_A being the approximant support size and is set to $r_A = 1.2d_r$ for all cases. These functions are approximated by Gaussian functions with equal amplitude and damping factors in x and y directions. Unfortunately, in the cases of circular resonator and dual polarized antenna, the computed input impedances are not in adequate agreement with MoM. This may be resulted from unsuccessful numerical de-embedding. Thus, in these cases, the monostatic radar cross section (RCS) computed by the proposed MFM and MoM are also provided to verify the validity of the method. For this purpose, the aforementioned structures are excited by x-polarized uniform plain wave. MoM results corresponding to S-parameter and RCS are computed by Agilent Momentum 2009 and FEKO suite 5.5, respectively. Finally, the plat form used is an Intel (R) Core (TM) 2 CPU with 4 GB RAM.

A. Linear resonator

Consider a 50 mm × 2.5 mm rectangular strip on a substrate with $\varepsilon_r = 1$ and $h = 0.794$ mm. The first resonance frequency of this structure can be analytically estimated to be 3 GHz. The node arrangement, BCs, current density distribution and the corresponding input impedance are depicted in Fig. 5. The computed results are in agreement with theoretical expectations.

(a)

(b)

(c)
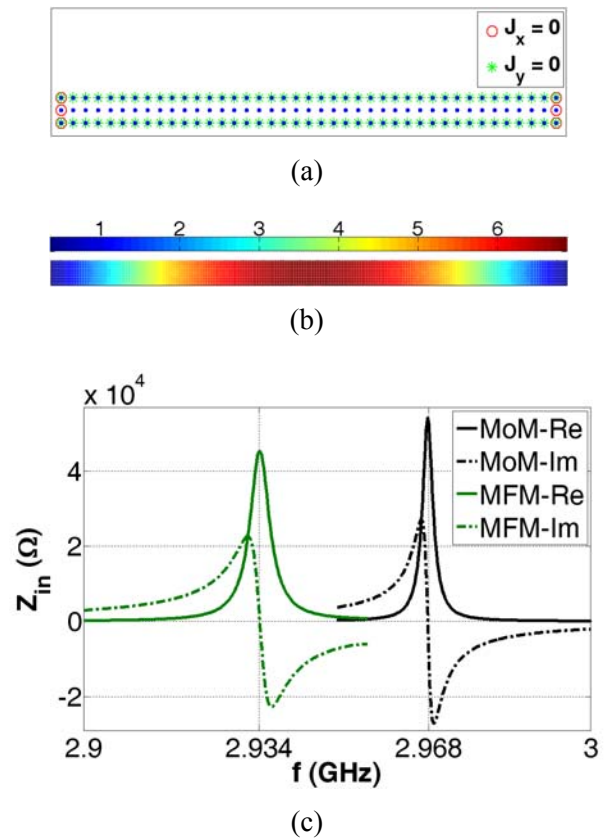
Fig. 5. Linear resonator for (a) nodal arrangement and BCs, (b) current density distribution, and (c) input impedance.

B. Proximity-coupled circular resonator

For verifying the applicability of the method to non rectangular geometries, consider a narrow ring, centered at the origin and fed by a 30 mm × 2.4 mm strip. The inner and outer radii of the ring are 7.5 mm and 10 mm, respectively. The ring and

the feed line are positioned 2 mm apart and are placed on a substrate with $\varepsilon_r = 1$ and $h = 1.6$ mm. The resonance frequency of the ring can be estimated to be 5.46 GHz. The nodal arrangement and BCs, current density distribution and the corresponding input impedance are depicted in Fig. 6. The computed results are in accordance with physical sense. Specially, Fig. 6 (b) shows how the EM energy is coupled to the ring at the resonance. Additionally, the capacitive nature of the feeding structure can be concluded from the imaginary part of input impedance. However, adequate agreement between MFM and MoM cannot be seen, which may be stem from unsuccessful numerical de-embedding. Thus, the normalized RCS is also computed by both of the methods and reported in Fig. 6 (d) for further validation of the proposed MFM.

C. Proximity-coupled antenna array

As the first radiating structure, consider a two-element array antenna, excited by proximity coupling technique. Each element consists of a 2.5 mm × 21.5 mm strip, perpendicularly fed by a $1.5\lambda_0$ × 2.5 mm line. The gap between the feed line and the strip is 1 mm, and the array elements are placed apart 6 mm. The substrate parameters are $\varepsilon_r = 1$ and $h = 1.6$ mm. The node arrangement and BCs for a single element, current density distribution at resonance and the corresponding $|S_{12}|$ are depicted in Fig. 7. For clearly visualizing the coupling of EM energy, the current density distribution is depicted in logarithmic scale.

D. Line-fed dual-polarized patch antenna

In contrast to previous cases, this case covers the microstrip discontinuity effect by connecting the feed lines to the radiating patch. For this purpose, a 10 mm ×10 mm patch is fed by two $1.5\lambda_0$ × 1.2 mm lines from its perpendicular sides. The lines are positioned at the center of each side. The substrate parameters are $\varepsilon_r = 1$ and $h = 0.794$ mm. The nodal arrangement and BCs, current density distribution at 13.1 GHz and the corresponding $|S_{12}|$ are depicted in Fig. 8. As in the case of circular resonator, the agreement between the MFM and MoM is not satisfactory. Thus, with the same reasoning, the RCS of the structure is computed by both of the methods and reported in Fig. 8 (d).

(a)

(b)

(c)

(d)
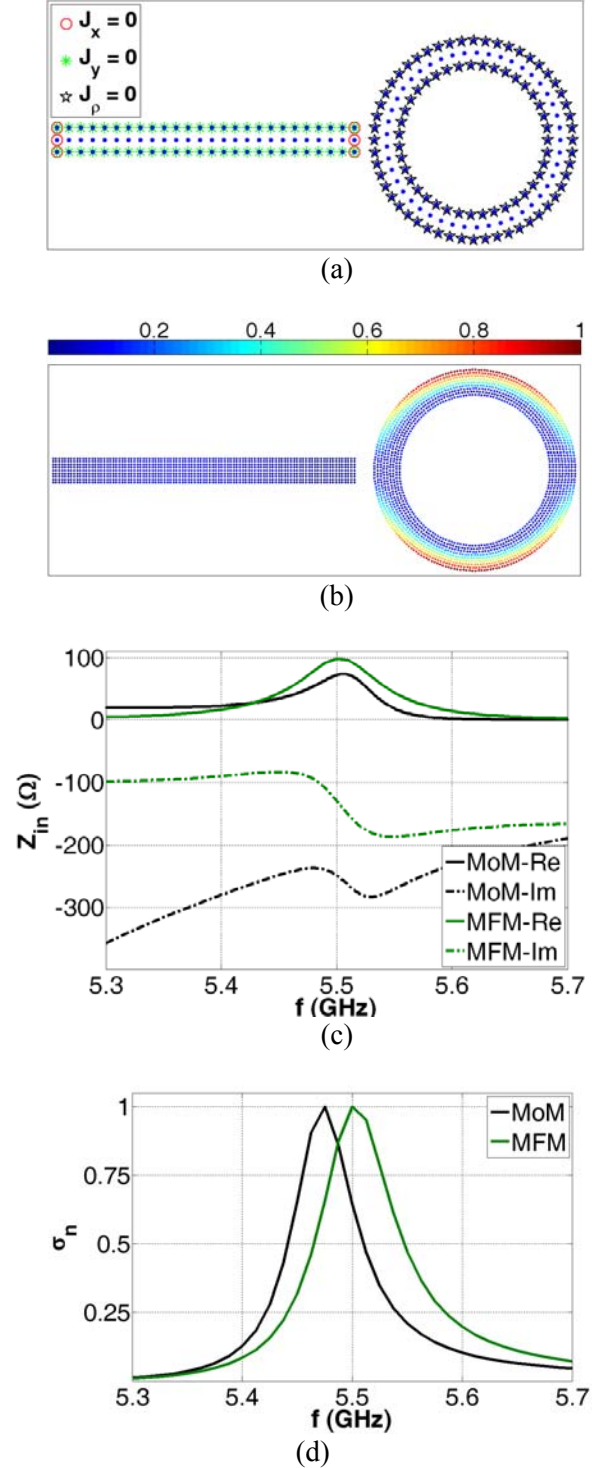
Fig. 6. Proximity-coupled circular resonator for (a) node arrangement and BCs, (b) current density distribution, (c) input impedance, and (d) normalized RCS.

(a)

(b)

(c)
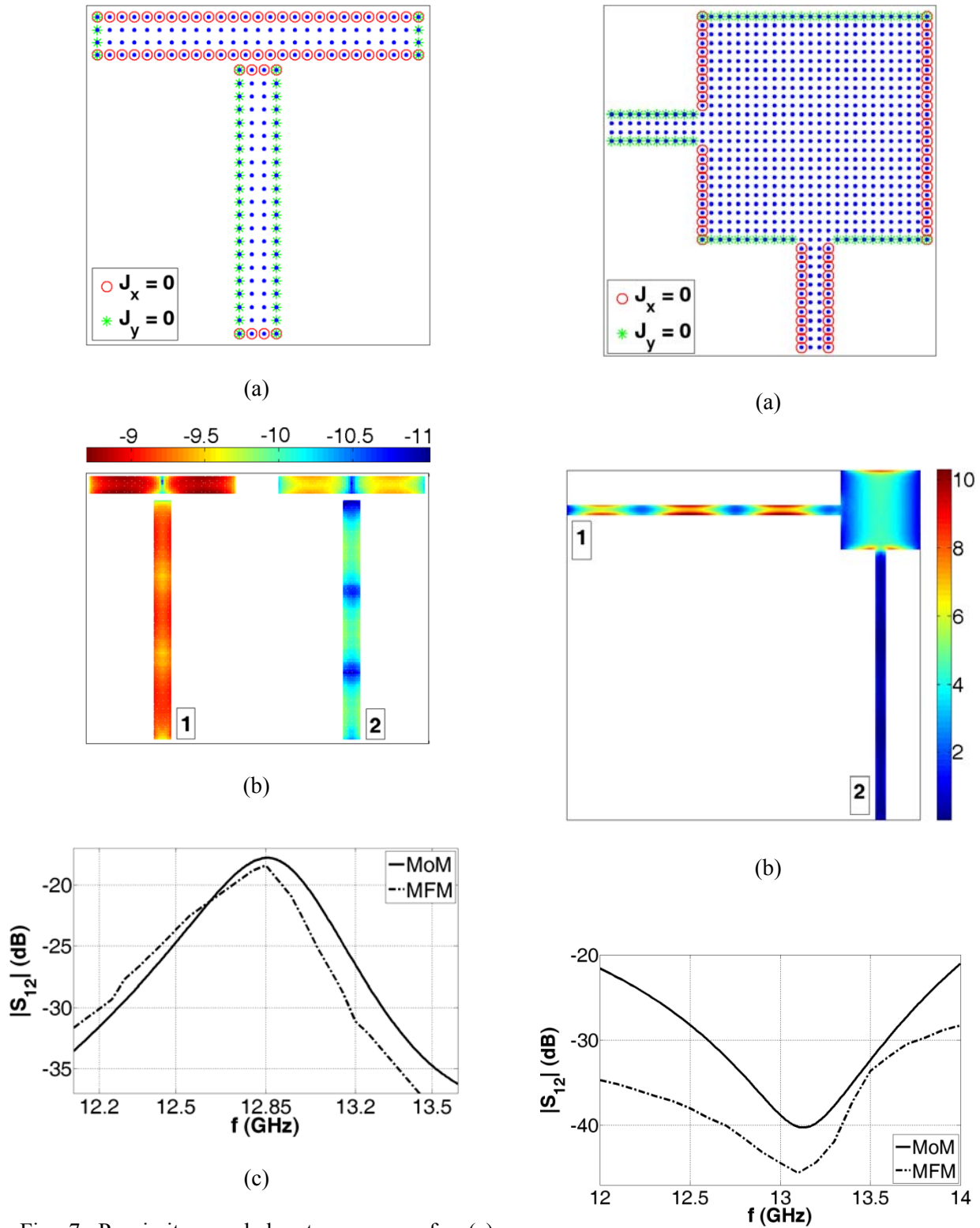
Fig. 7. Proximity-coupled antenna array for (a) node arrangement and BCs for a single element, (b) current density distribution, and (c) $|S_{12}|$.

(a)

(b)

(c)

(d)
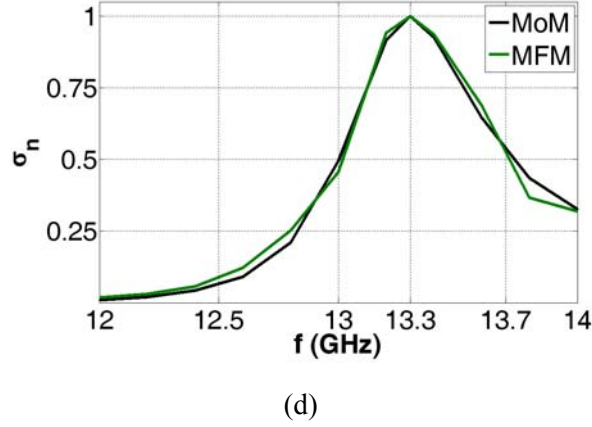
Fig. 8. Line-fed dual-polarized patch antenna for (a) node arrangement and BCs (the feeding lines are truncated for brevity.), (b) current density distribution, (c) $|S_{12}|$, and (d) normalized RCS.

E. Line-fed patch antenna

The final structure, is a 16 mm × 12.5 mm patch fed by a $1.5\lambda_0$ × 2.5 mm line, located on a substrate with $\varepsilon_r = 2.2$ and $h = 0.794$ mm. The line is positioned on the shorter side, 7 mm apart from the corner. Computing equation (16) is carried out based on [13]. The Sommerfeld integration path (SIP) in k_{z0} and k_ρ planes and the corresponding spectral domain functions at 18.7 GHz are depicted in Fig. 9. The matrix-pencil method (MPM) is used for expansion over complex exponentials [18]. The variables t, k_{z0}, k_ρ and functions R_{TE} and R_q are defined based on [12]. The nodal arrangement, BCs and the $|S_{11}|$ parameter in a wide frequency range are depicted in Fig. 10. The number of unknowns, N = 2M, and the simulation time of the proposed MFM and MoM are reported in Fig. 11. For this purpose, four nodes are used for discretizing the width of the feed line in MFM analysis, which makes the simulation valid up to about 20 GHz. Similarly, the mesh frequency in MoM is set to 20 GHz. The current density distributions at deeps of $|S_{11}|$ are depicted in Fig. 12.
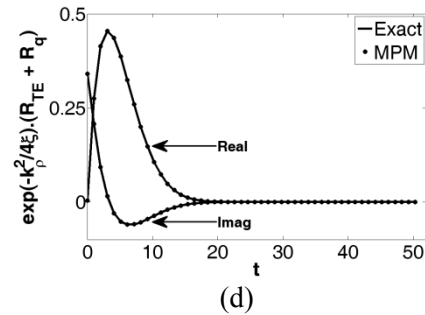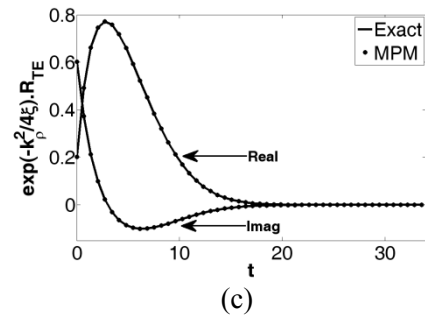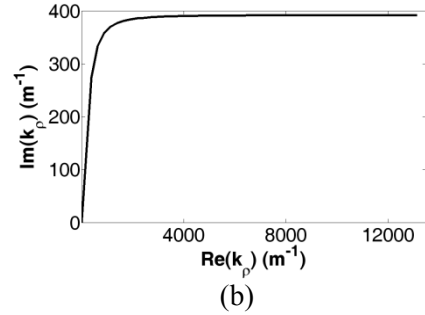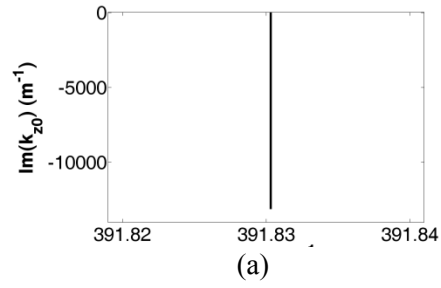
Fig. 9. Spectral domain curves at 18.7 GHz for (a) SIP in k_{z0}-plane, (b) SIP in k_ρ-plane, (c) spectrum corresponding to G_A^{xx}, and (d) spectrum corresponding to G_V.

(a)

(b)
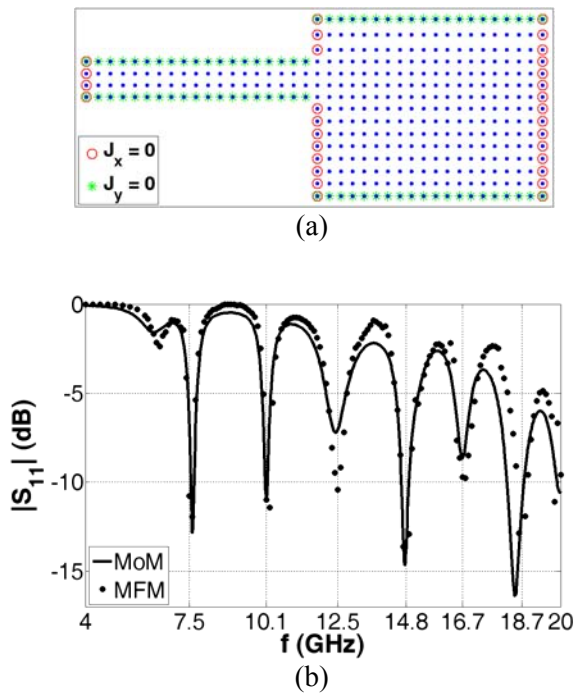
Fig. 10. Line-fed patch antenna for (a) node arrangement and BCs at 20 GHz and (b) $|S_{11}|$.

(a)

(b)
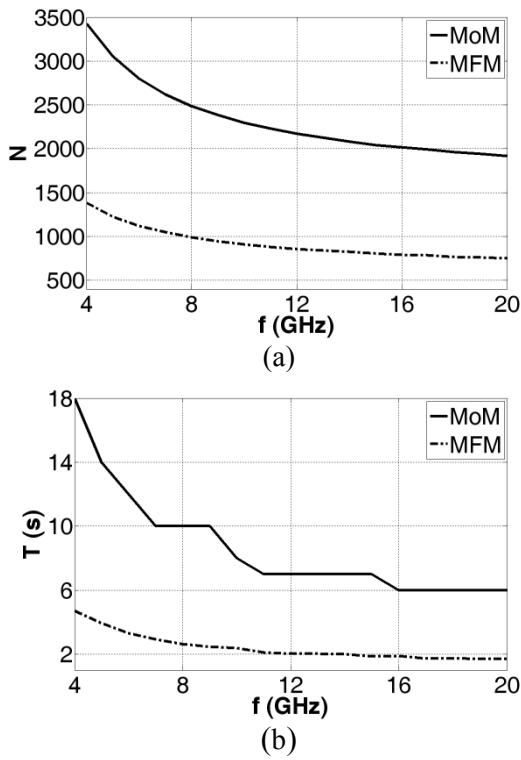
Fig. 11. Usage of computational resources for (a) number of unknowns (memory) and (b) time.
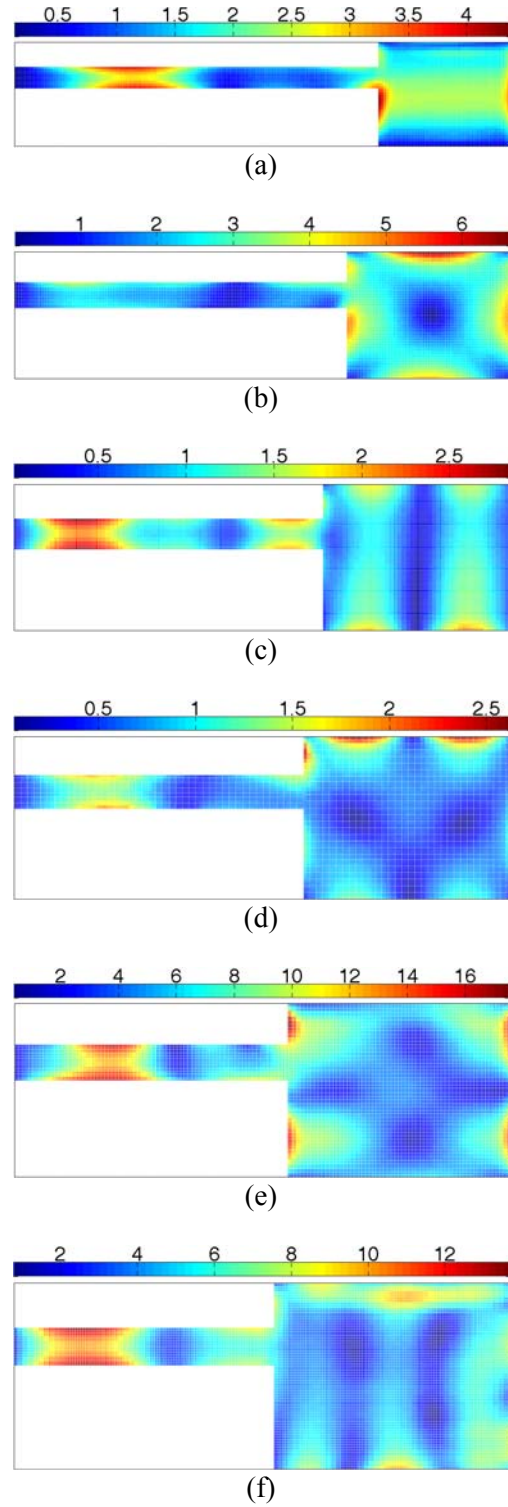
Fig. 12. Current density distribution of a line-fed patch antenna at (a) 7.5 GHz, (b) 10.1 GHz, (c) 12.5 GHz, (d) 14.8 GHz, (e) 16.7 GHz, and (f) 18.7 GHz (legends are scaled for each figure, independently.).

VIII. CONCLUSION

In this paper, five microstrip resonators/antennas are analyzed by the meshfree collocation method. The MPIE is used as the mathematical formulation of the problem. Guidelines are supplied for efficient meshless discretization leading to fast meshless integration-free solution. The proposed method is compared with MoM from the aspects of memory usage and simulation time which shows superior performance of the proposed MFM.

REFERENCES

[1] M. Zhang, L. Lingxia, P. Zhou, and X. Zhang, "A novel mesh-free method for electromagnetic scattering from a wire structure," *PIERS Online*, vol. 3, no. 6, pp. 774-776, 2007.

[2] D. Mirzaei and M. Dehghan, "A meshless based method for solution of integral equations," *Appl. Numer. Math.*, vol. 60, no. 3, pp. 245-262, 2010.

[3] W. L. Nicomedes, R. C. Mesquita, and F. J. S. Moreira, "An integral meshless-based approach in electromagnetic scattering," *COMPEL Int. J. Comput. Math. Elec. Elec. Eng.*, vol. 29, no. 6, pp. 1464-1473, 2010.

[4] W. L. Nicomedes, R. C. Mesquita, and F. J. S. Moreira, "2-D scattering integral field equation solution through an IMLS meshless-based approach," *IEEE Antennas Magn.*, vol. 46, no. 8, pp. 2873-2876, 2010.

[5] M. S. Tong and W. C. Chew, "A novel meshless scheme for solving surface integral equations with flat integral domains," *IEEE Trans. Antennas Propagat.*, vol. 60, no. 7, pp. 3285-3293, 2012.

[6] S. J. Lai, B. Z. Wang, and Y. Duan, "Meshless radial basis functions method for solving hallen's integral equation," *Appl. Comp. Electro. Society (ACES) Journal*, vol. 27, no. 1, pp. 9- 13, 2012.

[7] B. Honarbakhsh and A. Tavakoli, "Numerical solution of electromagnetic integral equations by the meshfree collocation method," *Appl. Comp. Electro. Society (ACES) Journal*, vol. 27, no. 9, pp. 706-716, 2012.

[8] R. F. Harrington, *Field Computation by Moment Methods*, New York: Macmillan, 1968.

[9] R. Mosig, "Arbitrary shaped microstrip structures and their analysis with a mixed potential integral equation," *IEEE Trans. Microwave Theory Tech.*, vol. 36, no. 2, pp. 314-323, 1988.

[10] G. R. Liu and Y. T. Gu, *An Introduction to MeshFree Methods and Their Programming*, Springer, 2005.

[11] D. Shepard, "A two dimensional interpolation function for irregularly spaced data," *Proc. 23rd Nat. Conf. ACM*, pp. 517-523, 1968.

[12] Y. L. Chow, J. J. Yang, D. G. Fang, and G. E. Howard, "A closed-form spatial Green's function for the thick microstrip substrate," *IEEE Trans. Microwave Theory Tech.*, vol. 39, no. 3, pp. 588-592, 1991.

[13] M. Yuan, T. K. Sarkar, and M. Salazar-Palma, "A direct discrete complex image method from the closed-form Green's functions in multilayered media" *IEEE Trans. Microwave Theory Tech.*, vol. 54, no. 3, pp. 1025-32, 2006.

[14] M. G. Duffy, "Quadrature over a pyramid or cube of integrands with a singularity at a vertex," *SIAM J. Numer. Ana.*, vol. 19, pp. 1260-1262, 1982.

[15] D. H. Schaubert, "A review of some microstrip antenna characteristics," D. M. Pozar and D.H. Schaubert, *Microstrip Antennas,* IEEE Press, 1995.

[16] J. C. Rautio, "A De-embedding Algorithm for Electromagnetics," *Int. J. MIMICAE*, vol. 1, no. 3, pp. 282-287, 1991.

[17] T. K. Sarkar, Z. A. Maricevic, and M. Kahrizi, "An accurate de-embedding procedure for characterizing discontinuities," *Int. J. MIMICAE*, vol. 2, no. 3, pp. 135-143, 1992.

[18] T. K. Sarkar and O. Pereira, "Using the matrix pencil method to estimate the parameters of a sum of complex exponentials," *IEEE Antennas Propagat. Mag.*, vol. 37, no. 3, pp. 48-55, 1995.

Babak Honarbakhsh was born in Tehran, Iran. He received his B.Sc. and M.Sc. degrees in Electrical Engineering from Amirkabir University of Technology where he is currently working toward his Ph.D. degree. His current research interest is numerical solution of electromagnetic problems by meshfree methods.

Ahad Tavakoli was born in Tehran, Iran, on March8, 1959. He received the B.S. and M.S. degrees from the University of Kansas, Lawrence, and the Ph.D. degree from the University of Michigan, Ann Arbor, all in electrical engineering, in 1982, 1984, and 1991, respectively. In 1991, he joined the Amirkabir University of Technology, Tehran, Iran, where he is currently a Professor in the Department of Electrical Engineering. His research interests include EMC, scattering of electromagnetic waves and microstrip antennas.